EPJ manuscript No.
(will be inserted by the editor)

Neutrino Interactions with Matter and the MiniBooNE anomaly

Luis Alvarez-Ruso and Eduardo Saul-Sala

Instituto de Física Corpuscular (IFIC) and Departamento de Física Teórica,
Consejo Superior de Investigaciones Científicas (CSIC) and Universidad de Valencia (UV)
E-46980 Paterna, Valencia, Spain

arXiv:2111.02504v1 [hep-ph] 3 Nov 2021

Abstract. The excess of electron-like events measured by MiniBooNE challenges our understanding of neutrinos and their interactions. We review the status of this open problem and ongoing efforts to resolve it. After introducing the experiment and its results, we consider the main experimental backgrounds and the related physics of neutrino interactions with matter such as quasielastic-like scattering and weak pion production on nucleons and nuclei. Special attention is paid to single photon emission in neutral current interactions and, in particular, its coherent channel. The difficulties to reconcile the MiniBooNE anomaly with global oscillation analysis is then highlighted. We finally outline some of the proposed solutions of the puzzle involving unconventional neutrino-interaction mechanisms.

1 The MiniBooNE short baseline anomaly

Neutrinos and antineutrinos are emitted in weak processes as flavor eigenstates. Once these are linear combinations of mass eigenstates, (anti)neutrinos change flavor with time because the phases of mass eigenstates evolve differently. Oscillation experiments detect charged leptons originated in (anti)neutrino charged-current (CC) interactions with a target. As an oscillation signature, appearance measurements search for charged leptons with flavors that differ from those of the originally produced neutrinos. MiniBooNE and the earlier LSND experiments belong to this category.

Precedent: LSND. The Liquid Scintillator Neutrino Detector (LSND) was illuminated by a beam of electron and muon (anti)neutrinos produced at Los Alamos National Laboratory from pion and muon decay at rest: $\pi^+ \to \mu^+ \nu_\mu$ followed by $\mu^+ \to e^+ \nu_e \bar{\nu}_\mu$. Electron antineutrinos were revealed by inverse beta decay $\bar{\nu}_e p \to e^+ n$. During its operation time between 1993 and 1998, the experiment found a signal excess of $87.9 \pm 22.4 \pm 6.0$ $\bar{\nu}_e$ events over the expected small intrinsic background [1]. In a simple model with two mass eigenstates, the oscillation probability is

$$P = \sin^2 2\theta \sin^2 \left(1.27 \Delta m^2 \frac{L}{E_\nu} \right) \tag{1}$$

with $\Delta m^2 = |m_1^2 - m_2^2|$ in units of eV^2, L the distance traveled by the neutrino in meters and E_ν its energy in MeV. Attributing the excess to $\bar{\nu}_\mu \to \bar{\nu}_e$ short ($\sim$ 30 m) baseline oscillations, an allowed region in the $(\sin^2 2\theta, \Delta m^2)$ plane is obtained with a best-fit $\Delta m^2 = 1.2$ eV^2 (see for instance Fig. 26 of Ref. [1]). Such a mass splitting, much larger than those obtained in the three-flavor paradigm established from solar, atmospheric, reactor and accelerator experiments [2], can be in principle accommodated by the introduction of sterile neutrinos that mix with the Standard Model (SM) flavors but do not couple directly to the weak bosons.

The MiniBooNE experiment. The MiniBooNE experiment [3] at Fermilab, was designed to detect electron (anti)neutrinos in a muon (anti)neutrino beam, with an average $L/E_\nu \sim 1$ m/MeV, similar to LSND, in order to test its earlier result.

The MiniBooNE detector is a 12.2 m diameter spherical tank filled with 818 tonnes of mineral oil, CH_2, with 1280 photomultiplier tubes to collect Cherenkov light produced by charged particles emitted in the interaction processes. The neutrino flux directed to MiniBooNE is produced by meson (mostly pion) decay in flight at the Fermilab Booster neutrino beamline, with a baseline of 541 m. The 20 times larger baseline compared to LSND entails a proportionally larger $E_\nu \sim 500$ MeV to keep $L/E_\nu \sim 1$ m/MeV. The proton beam is directed to a beryllium target, where the secondary meson beam is produced. Using magnetic fields, one of the components of the meson beam can be selected to obtain a beam of predominantly neutrinos or antineutrinos. For example, by keeping the π^+ muonic neutrinos are favored by their decay, $\pi^+ \to \mu^+ + \nu_\mu$. The largest ν_μ and $\bar{\nu}_\mu$ components of the fluxes at the MiniBooNE detector in both neutrino and antineutrino modes are shown in Fig. 1. Electron (anti)neutrino components are orders of magnitude smaller [4]. It can be seen that the ν_μ contamination in antineutrino mode is relatively larger than the $\bar{\nu}_\mu$ one in neutrino mode.

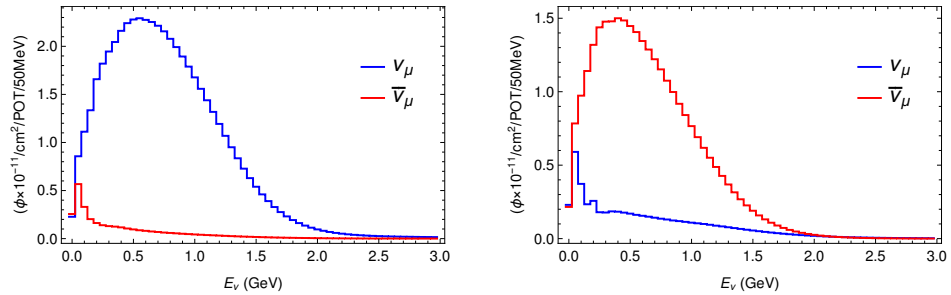


Fig. 1. Leading components of the neutrino flux at MiniBooNE in neutrino (left) and antineutrino (right) modes [4].

The experiment searched for electron-like charged-current quasielastic (CCQE) events originated in $\nu_e\, n \to e^-\, p$ ($\bar{\nu}_e\, p \to e^+\, n$) interactions in neutrino (antineutrino) mode. Data collected between 2002 and 2012 for 6.46×10^{20} protons on target (POT) in neutrino mode and 11.27×10^{20} POT in antineutrino mode showed an excess of events over the predicted background in both cases [5]. The distribution of these events are shown in Fig. 2 as a function of $E_\nu^{\rm QE}$, defined as the energy of the incoming neutrino reconstructed from the energy E_e and scattering angle θ_e of the final $e^\pm$ assuming that the interaction took place on a single non-interacting nucleon bound with a constant

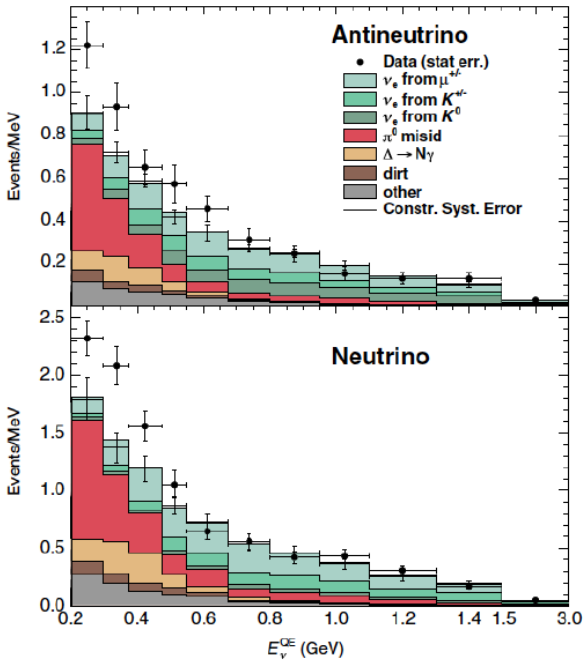


Fig. 2. Results of the MiniBooNE experiment in both antineutrino (upper panel) and neutrino (lower panel) modes [5]. The distribution of electron-like events (oscillation candidates) as a function of $E_\nu^{\rm QE}$ is shown together with background estimates.

binding energy

$$E_\nu^{\rm QE} = \frac{2M'_{n(p)}E_e - M'^2_{n(p)} + M^2_{p(n)} - m_e^2}{2(M'_{n(p)} - E_e + \sqrt{E_e^2 - m_e^2}\cos\theta_e)}\,, \tag{2}$$

where $M'_{n(p)} = M_{n(p)} - E_B$ with $E_B = 34$ MeV. The excess is concentrated at $200 < E_\nu^{\rm QE} < 475$ MeV. The lower $E_\nu^{\rm QE}$ limit is dictated by the ability to reconstruct reliably ν_μ Cherenkov rings with visible energies greater than 140 MeV. From 2012 to 2019, data has been further collected in neutrino mode, reaching 18.75×10^{20} POT [6], confirming the original results (compare Fig. 9 of Ref. [6] to the lower plot in Fig 2 from Ref. [5]).

An oversimplification of nuclear structure and reaction dynamics underlies in the experimentally adopted definition of $E_\nu^{\rm QE}$ given above. It is known that nucleons in the nucleus are not at rest but undergo Fermi motion and, when knocked out from the nucleus, propagate in density and momentum-dependent mean field potentials (see for instance the discussion in section 2.5 of Ref. [7]). Moreover, external probes can interact with nucleon pairs or, at low energy and momentum transfers, collective modes can be excited [8]. Several independent calculations have established that a sizable fraction of the CCQE-like dataset collected by MiniBooNE originates in interactions with nucleon pairs [9–12]. This introduces a bias in the migration matrix form $E_\nu^{\rm QE}$ to the true E_ν [13, 14], as can be appreciated in Fig 3 taken from Ref. [13]. Besides Fermi smearing, low energy tails due to scattering off nucleon pairs are present at all but the lowest $E_\nu = 200$ MeV. Additional strength in the tail arises from CC pion production events followed by pion absorption in the nucleus [15].

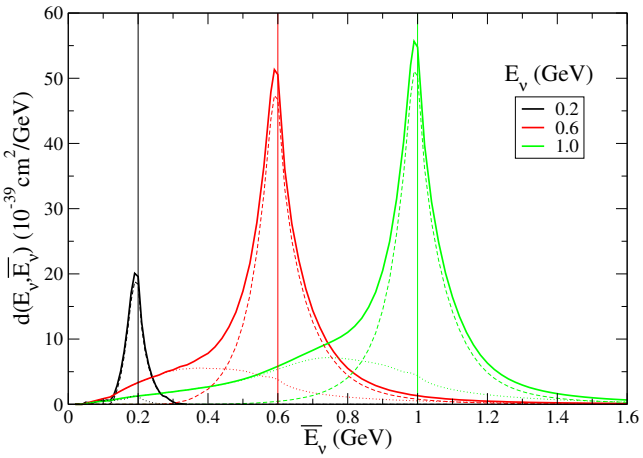


Fig. 3. Spreading of $E_\nu^{\rm QE}$ (denoted $\bar{E}_\nu$) in ν_e-^{12}C CCQE-like scattering due to nuclear effects, for three fixed true E_ν [13].

While the presence of such a bias should not cast doubts on the existence of the electron-like excess itself, it might influence its explanation. In particular, if interpreted in terms of $\nu_\mu \to \nu_e$ oscillations, an unaccounted mismatch between the true E_ν, upon which the oscillation probabilities depend, and $E_\nu^{\rm QE}$ will alter the determination of oscillation parameters. For tests of alternative explanations of the MiniBooNE anomaly not involving neutrino oscillations, a representation of the excess of events in terms of the visible energy and angle between the reconstructed electron and the beam direction (see Figs. 7, 8 and 13 of Ref. [6]) is better suited.

2 Backgrounds at MiniBooNE

As apparent from Fig. 2, the mere existence, size and kinematic distribution of the MiniBooNE excess of events critically relies on the proper determination of electron-like backgrounds which, in the absence of a near detector, are determined using MiniBooNE data. A brief updated description of these backgrounds has been presented in Ref. [16]; here we revisit them from a more theoretical perspective.

Intrinsic electron-(anti)neutrino background. This background comes from in-flight decays of muons and kaons. The $\nu_e\,(\bar{\nu}_e)$ component in the flux from muon decays is directly related to the observed $\nu_\mu\,(\bar{\nu}_\mu)$ events due to the common origin in pion decays. The fraction from kaon decays is constrained by fits to kaon production data and by high-energy data measured at the SciBooNE detector [17]. The number of CCQE-like events at the detector and their kinematic distributions are determined by the experiment's Monte Carlo, tuned to measured ν_μ CCQE-like scattering on ^{12}C. However, the Monte Carlo simulation does not take into account multinucleon-events. This is a potential source of systematic uncertainty as the ν_μ/ν_e cross section ratio for scattering on nucleon pairs is different than for CCQE scattering. The impact of this difference on the shape (not in the total number of $\nu_e\,(\bar{\nu}_e)$, which is normalized to the MiniBooNE prediction) of the predicted intrinsic $\nu_e\,(\bar{\nu}_e)$ background was studied in Ref. [18]. After this correction, the obtained background, shown in Fig. 4, is consistent with the original MiniBooNE estimate but shows an enhancement in the low energy bins, which is stronger in neutrino mode.

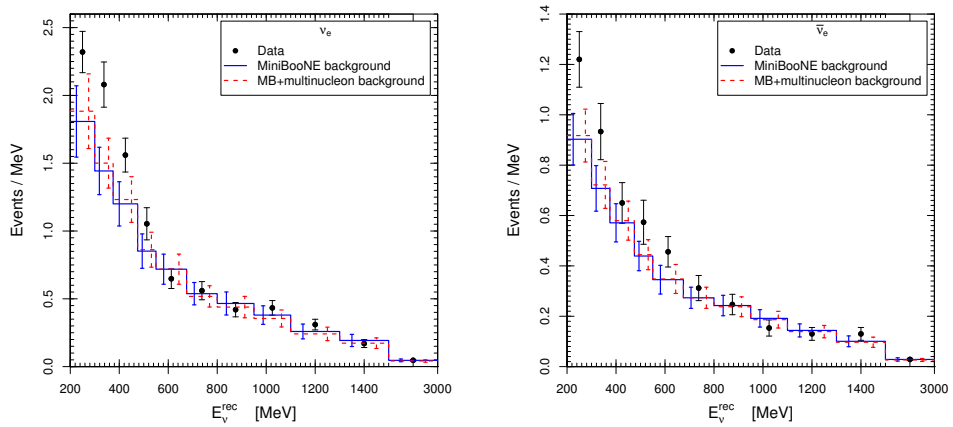


Fig. 4. Electron-like background at MiniBooNE taking into account multinucleon contributions [18] compared to the original estimate.

External events. Photons produced outside the detector can give a signal inside without triggering a veto. As Cherenkov detectors cannot distinguish between photons and electrons, such signals are indistinguishable from CCQE-like interactions of electron (anti) neutrinos. These *dirt* background events are difficult to estimate as the outside surroundings of the detector are incompletely simulated. For this purpose, MiniBooNE isolates events near the edge of the detector and pointing towards the detector center. Furthermore, timing information (see Fig. 5 taken from Ref. [6]) shows that the event excess peaks in the 8 ns window associated with beam bunch time, as expected from neutrino events in the detector. The *dirt* event prediction is tested by the correct description of data taken off-phase with respect to the beam.

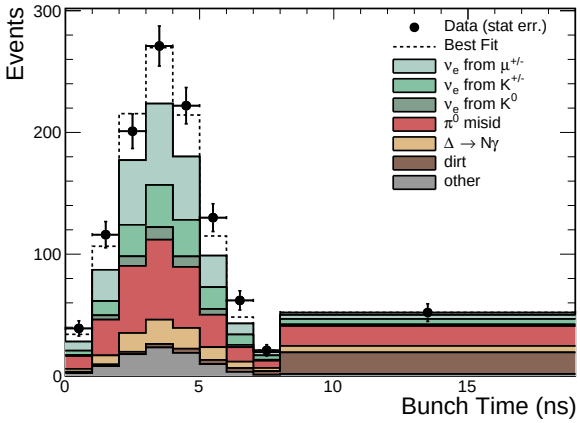


Fig. 5. The bunch timing for data events in neutrino mode compared to the expected background [6].

Neutral-current π^0 background. The production of neutral pions by neutral current (NC) interactions of (anti)neutrinos of all flavors with nuclei in the detector material

$\nu(\bar{\nu})\,A \to \nu(\bar{\nu})\,X\,\pi^0$ (the hadronic final state X contains any number of nucleons and nuclear fragments but no mesons or photons) is a source of electron-like background events in Cherenkov detectors such as MiniBooNE or Super Kamiokande when one of the photons from the $\pi^0 \to \gamma\,\gamma$ decay is unresolved. In the case of MiniBooNE this background, represented in red in Fig. 2, is the largest at low $E_\nu^{\rm QE}$, where the excess of events is present.

A reliable simulation of this background should tackle (at least to some extent) the challenging problem of weak pion production in nuclei. A basic ingredient is a realistic model for neutrino-induced pion production on single nucleons. Although this process is dominated by the excitation of baryon resonances and their subsequent decay into πN, there are also non-resonant mechanisms which coexist and interfere with resonant ones. At MiniBooNE energies, the largest contribution is mediated by the $\Delta(1232)$ resonance. Isospin considerations imply that the $\Delta(1232)$ is dominant for $\nu_l p \to l^-\,p\,\pi^+$ and $\bar{\nu}_l n \to l^+\,n\,\pi^-$ but the relative importance of non-resonant and N^*-mediated amplitudes is larger for NC reaction channels [1]. While at low energy and momentum transfers, weak pion production can be systematically studied using Chiral Perturbation Theory [19], the kinematic range probed by neutrino interactions at MiniBooNE demands a more phenomenological approach. Phenomenological models for weak meson production rely on symmetries to constrain the parameters with precise and abundant non-neutrino data. Owing to isospin symmetry, the form factors that characterize the vector part of the weak current can be extracted from pion electroproduction data [20]. On the other hand, the partial conservation of the axial current (exact only in the chiral limit but still a good approximation thanks to the lightness of pions) allows to relate the axial current at zero four-momentum transfer squared (q^2) to the pion-nucleon scattering amplitude, which is also well known experimentally. Such a connection with pion electroproduction and pion-nucleon scattering data is present in all models but is most extensively exploited by the dynamical model in coupled channels of Ref. [21]. What remains unconstrained by non-neutrino data is the q^2 dependence of the axial current form factors, on which only limited information can be extracted from bubble-chamber data on pion production induced by neutrinos on deuterium, taken at Argonne and Brookhaven National Laboratories (ANL and BNL) [22].

When pions are produced on nuclear targets as in all modern neutrino experiments, including MiniBooNE, the presence of the nuclear medium poses additional challenges for the reaction modeling. Given the prevalent role of the $\Delta(1232)$ excitation in pion production, it is not surprising that the in-medium modification of the Δ propagator is very important. The main effect is the increase of the $\Delta(1232)$ width (broadening) by many body processes: $\Delta\,N \to N\,N$, $\Delta\,N \to N\,N\,\pi$, $\Delta\,N\,N \to N\,N\,N$. In their way out of the nucleus, pions undergo final state interactions (FSI). They can be absorbed, change their energy, angle and charge. In particular, in NC interactions, there is a shift of strength from the largest π^0 production channel to the $\pi^\pm$ ones via charge-exchange FSI: $\pi^0\,p \to \pi^+\,n$ and $\pi^0\,n \to \pi^-\,p$ [23].

In order to minimize the impact of uncertainties and mismodeling on the NCπ^0 background determination, the MiniBooNE experiment relies on its own measurement of the NCπ^0 reaction [24] to tune the simulation. One should nonetheless bear in mind that the theoretical description of MiniBooNE pion production data has encountered difficulties. The left panel of Fig. 6 shows that the Giessen Boltzmann-Uehling-Uhlenbeck transport model (GiBUU) fails to reproduce the experimental π^0 spectrum for pion momenta between 200 and 500 MeV/c [25]. The shape disagree-

[1] The $W^+\,p \to \Delta^{++} \to p\,\pi^+$ matrix element is proportional to Clebsch-Gordan coefficient $(1/2\,1/2\,1\,1|3/2\,3/2)^2 = 1$ while for $Z^0\,p \to \Delta^+ \to p\,\pi^0$ one has $(1/2\,1/2\,1\,0|3/2\,1/2)^2 = 2/3$.

ment apparent in Fig 6 (left) is in contrast with the result of the GiBUU model for the CC$\pi^{\pm}$ (mostly π^{+}) reaction compared to MINERvA data. The right panel of Fig 6 is adapted from Fig. 1 of Ref. [26]. The band between the two solid lines represent the uncertainty from ANL and BNL data [26] [2].

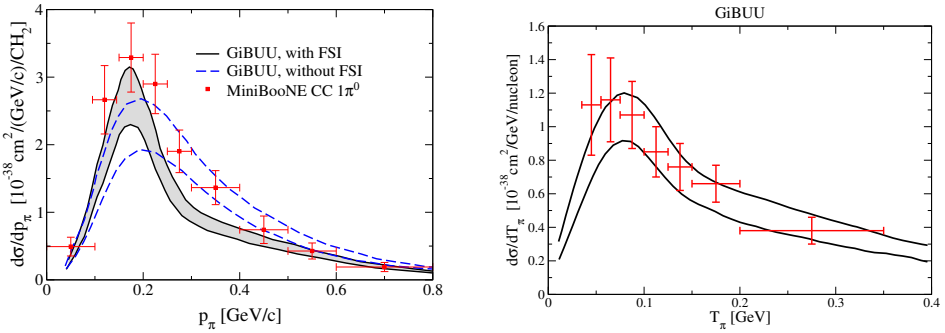


Fig. 6. Predictions from the GiBUU transport model for weak pion production. Left: the CC1π^0 differential cross section on CH_2 folded with the ν_μ flux at the MiniBooNE detector as a function of the pion momentum [25] compared to data from Ref. [28]. Right: differential cross section for CC$\pi^{\pm}$ on CH averaged over the MINERvA low-energy flux as a function of the pion kinetic energy [26] compared to data from Ref. [29].

One is tempted to attribute the different scenarios displayed by Fig 6 to the differences in the corresponding neutrino fluxes. The flux at MiniBooNE peaks at nearly 700 MeV (Fig. 1) while the MINERvA low-energy one does close to 3 GeV. However, the GiBUU model also describes well pion production at T2K (Figs. 2 and 3 of Ref. [30]), whose flux peaks at a around the same energy as the MiniBooNE one. Moreover, according to the study of Ref. [31], there is a strong correlation among the two data sets (at least for charged pions) in spite of the flux differences. Using the NuWro generator, the authors of Ref. [31] have obtained that the ratio

$$R(T_\pi) = \frac{(d\sigma/dT_\pi)_{\text{MINERvA, CC}\pi^{\pm}}}{(d\sigma/dT_\pi)_{\text{MiniBooNE, CC}\pi^{+}}} \approx 2 \tag{3}$$

as can be seen in Fig. 7, adapted from Ref. [31]. In both experiments, the dominant contribution comes from the $\Delta(1232)$ region. The cut in the reconstructed invariant mass $W_{\text{rec}} \equiv \sqrt{m_N^2 + 2m_N q_0 + q^2} < 1.4$ GeV is applied in the MINERvA analysis [29] using measured lepton kinematics and calorimetry. It quenches the contribution from higher invariant masses although the cut is not sharp, and the Δ peak is shrunk from its maximum on [26]. As shown in Fig. 7, the correlation obtained in Ref. [31] with NuWro is absent in the data.

Even if established specifically for charged pions, this unresolved tension could have implications for the determination of this important background in the MiniBooNE oscillation measurement. Indeed, it would be interesting to study the NCπ^0 background prediction based on a pion production model, like GiBUU, that explains MINERvA data but such an exercise requires a simulation of the MiniBooNE detector. It should be however added that the NCπ^0 background has more events near the

[2] This band would be narrower and closer to the lower end if the reanalyzed ANL and BNL data of Ref. [27] had been used.

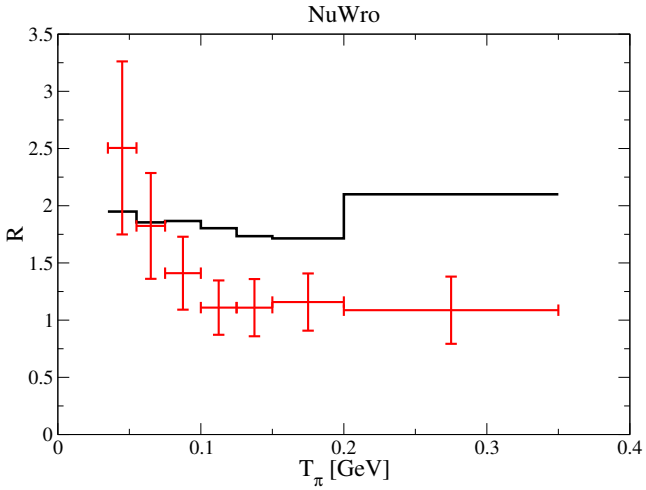


Fig. 7. Ratio of $d\sigma/dT_\pi$ from MiniBooNE and MINERvA [Eq. (3)], and the corresponding NuWro predictions [31].

edge of the fiducial volume because of the greater chance that one of the decay photons leaves the detector, while electron events are more homogeneously distributed over the detector volume. In Ref. [6], the MiniBooNE experiment used this feature of the radial distribution of event vertices to show that an explanation of the anomaly in terms of unaccounted NCπ^0 electron-like events or, in general, due to entering or exiting photons, is disfavored.

Single-gamma background. As previously stated, Cherenkov detectors like MiniBooNE misidentify single photon tracks as electrons. Apart from the sources discussed above, such single photons can be produced in NC interactions, NC1γ, inside the fiducial volume. Although it is not exactly the case (see below), MiniBooNE assumes that the NC1γ events come entirely from $\Delta(1232)$ radiative decay: $\Delta \to N\,\gamma$ and constrains it using the NCπ^0 data [24] and the NC1γ/NCπ^0 ratio, taken to be 0.0091 ± 0.0013 [6]. The derivation of this number is sketched in Ref. [6] and reproduced here: the $\Delta(1232)$ contribution to the NCπ^0 event sample is 52.2% on ^{12}C and 15.1% on H_2; the $\Delta \to N\,\pi^0$ fraction is 2/3 and the probability that a pion escapes from ^{12}C is estimated to be 62.5%. Finally, the Δ radiative branching fraction is 0.60% (0.68%) on ^{12}C (H_2). Altogether, for CH_2 one has $0.151/(2/3) \times 0.0068.5 + 0.522/(2/3)/0.625 \times 0.0060 = 0.0091$. The total uncertainty on this ratio is 14.0% (15.6%) in neutrino (antineutrino) mode. Estimated in this way, the NC1γ one represents the second largest background in the kinematic region where the excess is found.

The fact that the single-gamma background is only indirectly determined, while only upper limits are experimentally available [32, 33] has stimulated the theoretical activity to model the NC1γ reaction on nucleons and nuclei. The following section summarizes these efforts.

3 Theoretical description of photon emission in NC interactions in the Standard Model

Photon emission induced by NC interactions can take place on single nucleons

$$\nu(\bar{\nu})\, N \to \nu(\bar{\nu})\, \gamma\, N\,, \tag{4}$$

and on nuclear targets

$$\nu(\bar{\nu})\, A \to \nu(\bar{\nu})\, \gamma\, X \tag{5}$$

$$\nu(\bar{\nu})\, A \to \nu(\bar{\nu})\, \gamma\, A \tag{6}$$

via incoherent [Eq. (5)] or coherent [Eq. (6)] scattering.

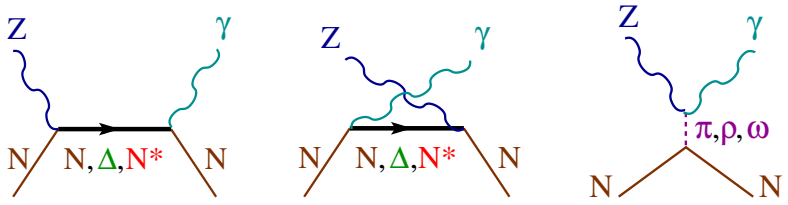


Fig. 8. Feynman diagrams for NC photon emission considered in the literature. The first two diagrams stand for direct and crossed baryon pole terms with nucleons and baryon resonances $\Delta(1232)$, $N^*(1440)$, $N^*(1520)$, $N^*(1535)$ in the intermediate state. The third diagram represents t-channel meson (π, ρ, ω) exchange contributions.

Theoretical models for the reaction of Eq. (4) in the few-GeV region have been developed in Refs. [34–36]. These calculations incorporate s- and u-channel amplitudes with nucleons and $\Delta(1232)$ in the intermediate state, Fig. 8. The structure of nucleon pole terms at threshold is fully determined by the symmetries of the SM. The extension towards higher energy and momentum transfers, required to predict cross sections at MiniBooNE, is performed by the introduction of phenomenologically parametrized weak and electromagnetic form factors. The same strategy has been followed for the resonance terms. The cross sections on elementary targets obtained in Ref. [36] are reproduced in Fig. 9. They show that the $\Delta(1232)$ excitation followed by radiative decay is the dominant mechanism, as correctly assumed by MiniBooNE, and in agreement with the findings of Refs. [34, 35]. Nonetheless, the contribution from the $N(1520)3/2^-$ on proton targets is sizable above $E_\nu \sim 1.5$ GeV, while $N(1440)1/2^+$ and $N(1535)1/2^-$ are negligible. The pion-pole mechanism, which originates from the $Z^0\gamma\pi$ vertex, fixed by the axial anomaly of QCD, is nominally of higher order [35] and, indeed, gives a very small contribution to the cross section. Among terms with heavier meson t-channel exchange, the ω one was proposed as a solution for the MiniBooNE anomaly [37] because of the rather large (although uncertain) couplings and the ω isoscalar nature, which enhances its impact on the coherent reaction of Eq. (6). However, actual calculations found this contribution small compared to $\Delta(1232)$ excitation [34, 38].

The incoherent NCγ reaction on nuclear targets, Eq. (5), has been studied in Refs. [36, 39] using the relativistic local Fermi gas approximation to take into account Fermi motion and Pauli blocking. The broadening of the Δ resonance in the medium has also been incorporated using a spreading potential in Refs. [39, 40], while Ref. [36] uses the parametrization of the imaginary part of the in-medium Δ selfenergy as

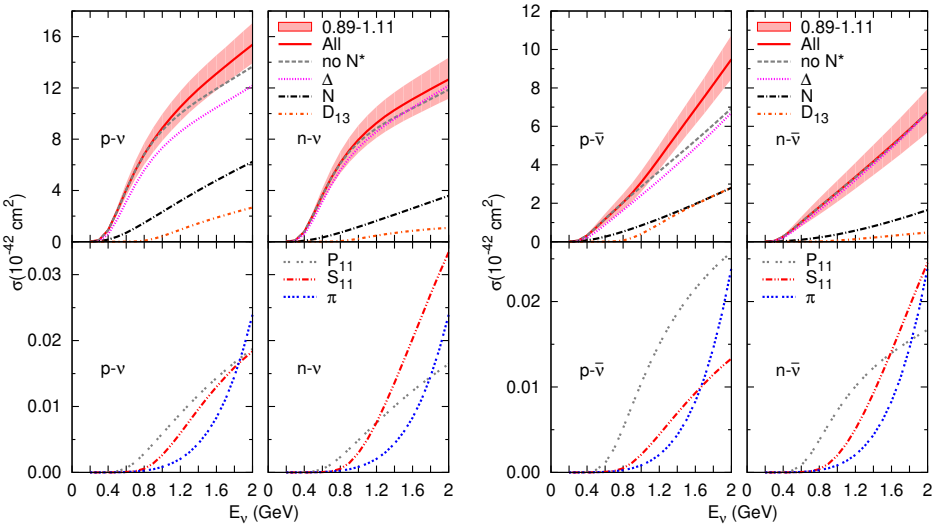


Fig. 9. NC1γ cross sections on protons and neutrons as a function of the (anti)neutrino energy according to the model of Ref. [36]. The error bands in the full-model results (solid lines) represent the uncertainty in the leading axial $N\Delta$ coupling denoted as $C_5^A(0)$.

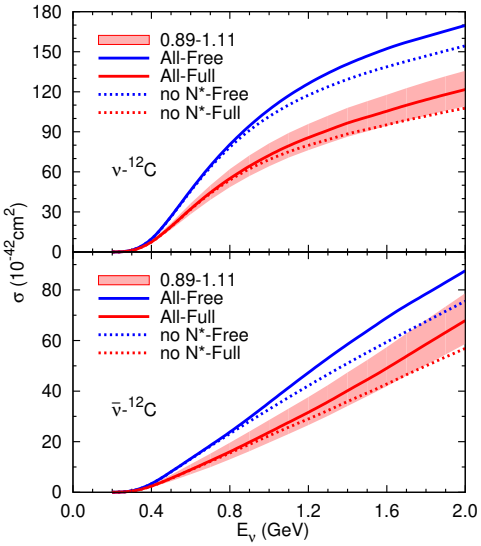


Fig. 10. Neutrino (top) and antineutrino (bottom) incoherent photon emission cross sections on ^{12}C. Curves denoted as "Free" do not include any nuclear correction while those labeled as "Full" take into account Pauli blocking, Fermi motion and the in medium Δ resonance broadening. The error bands show the uncertainty on the full model from $C_5^A(0)$.

a function of the local nuclear density derived in Ref. [41]. The neglect of nuclear medium corrections is a poor approximation: by taking into account Fermi motion and Pauli blocking, the cross section already goes down by more than 10%. With the full model the reduction is of the order of 30% as can be seen in Fig. 10 taken from Ref. [36]).

The NCγ model outlined above has been applied to calculate the number and distributions of single photon events at MiniBooNE [42], using the available information about the detector mass and its composition (CH_2), the number of POT, [5], flux prediction (Fig. 1) and photon detection efficiency [43]. As shown in Fig. 11 taken from Ref. [42], yields from the incoherent channel are the largest ones. Those from the coherent channel and the reaction on protons, which are comparable, are smaller but significant.

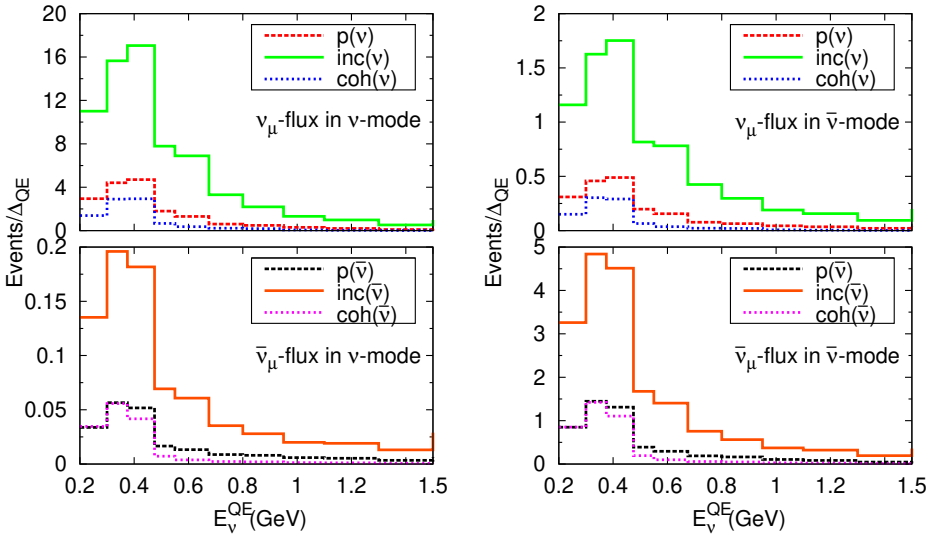


Fig. 11. Predicted distribution of NC1γ events at MiniBooNE as a function of $E_\nu^{\rm QE}$ for the ν_μ (top) and $\bar{\nu}_\mu$ (bottom) MiniBooNE fluxes in the ν(left) and $\bar{\nu}$ (right) modes [42] calculated with the model of Ref. [36].

The sum of all contributions in Fig. 11 are shown in Fig. 12. The error bands correspond to a 68 % confidence level according to the error budget in Table 1 of Ref. [42] and is dominated by the uncertainty in the $C_5^A(0)$ $N\Delta$ axial coupling. The comparison with the MiniBooNE estimate described above shows a good agreement: the shapes are similar and the peak positions coincide. The largest discrepancy is observed in the lowest energy bin. In the two bins with the largest number of events, the two calculations are consistent within our errorbars. The overall agreement is also good in comparison to the result of Zhang and Serot [40].

We should warn the reader that all the results shown in this section were obtained assuming a value of $C_5^A(0) = 1.00 \pm 0.11$ determined in a fit to $\nu_\mu d \to \mu^- p \pi^+ n$ BNL and ANL data in the Δ region [22]. However, a re-analysis of these data with an improved version of the weak pion production model obtained a higher $C_5^A(0) = 1.18 \pm 0.07$, which is also in excellent agreement with the off-diagonal Goldberger-Treiman relation for the $N\Delta$ transition. This change would cause an increase in the NC1γ cross section and in the number of events predicted at MiniBooNE, leading to a better agreement with the MiniBooNE determination in the first bin, but overestimating it in most bins. This is, after all, not surprising given the fact that theory takes into account NC1γ mechanisms that are unaccounted by MiniBooNE. In any case, such an increase would be insufficient to explain the anomaly. The same conclusion applies to the study of Ref. [44] where a two-nucleon Δ mediated meson exchange mechanism

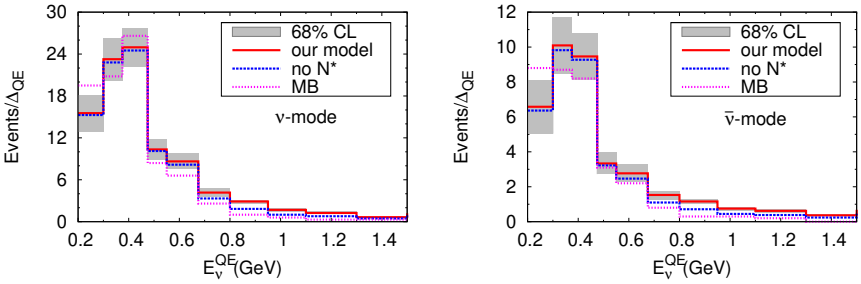


Fig. 12. $E_\nu^{\rm QE}$ distributions of total NCγ events for the ν (left) and $\bar{\nu}$ (right) modes. The "MB" histograms display the MiniBooNE estimates [43].

was considered for the average of NC neutrino and antineutrino cross sections. Its contribution appears to be significant but, as expected, smaller (a factor of around 9 at $E_\nu = 500$ MeV) than the single nucleon mechanisms discussed above.

As stated above, the coherent reaction channel, Eq. 6, is responsible for a small but non-negligible fraction of the NC1γ events at MiniBooNE. It is particularly important for antineutrinos and in the forward direction (see Fig. 3 of Ref. [42]). Furthermore, coherent NC1γ emission appears as a background to some of the proposed explanations of the MiniBooNE event excess outlined in Sec. 4, which involve physics beyond the SM and can be tested at Fermilab by the Short Baseline Neutrino Detector (SBND) or by MINERvA. For these reasons we dwell longer on the theoretical description of this process.

Coherent photon emission in NC interactions In the process of Eq. 6, diagrammatically illustrated in Fig. 13, a neutrino with four-momentum $k \equiv (E_\nu, \vec{k})$ interacts with a nucleus of four-momentum $P \equiv \left(E, \vec{P}\right)$. After the interaction, the nucleus remains in the ground state, changing only its four-momentum to $P' \equiv \left(E', \vec{P}\,'\right)$, while the neutrino does to $k' \equiv (E'_\nu, \vec{k}\,')$. The four-momentum of the emitted photon is $k_\gamma \equiv \left(E_\gamma, \vec{k}_\gamma\right)$ and the one transferred by the neutrino is $q = k - k'$. In the Laboratory frame $P = (M_A, 0)$, where M_A denotes the target mass. Under the assumption that the recoil kinetic energy of the outgoing nucleus $(E' - M_A) \ll M_A$, energy conservation implies that $q_0 = E_\gamma$.

In the framework adopted here, which is adapted from Refs. [45, 46] for neutrino-induced coherent pion production reactions, the cross section in the Laboratory frame is given by

$$\frac{d\sigma}{dE_\gamma d\Omega_\gamma d\Omega_{k'}} = \frac{1}{8}\frac{1}{(2\pi)^5}\frac{E'_\nu E_\gamma}{E_\nu}|\overline{\mathcal{M}}|^2 \,. \tag{7}$$

Owing to the coherence, the nucleon wave function inside the nucleus remains unchanged. Hence, after summing the elementary $ZN \to N\gamma$ amplitudes over all nucleons, one obtains the nuclear density distributions of protons and neutrons, $\rho_{p,n}(r)$. The absolute value of the amplitude squared can be cast as

$$|\overline{\mathcal{M}}|^2 = -\frac{G_F^2}{2} e^2 L_{\alpha\beta}\, g_{\mu\nu}\, (R^{\mu\alpha})^\dagger\, R^{\nu\beta} \,, \tag{8}$$

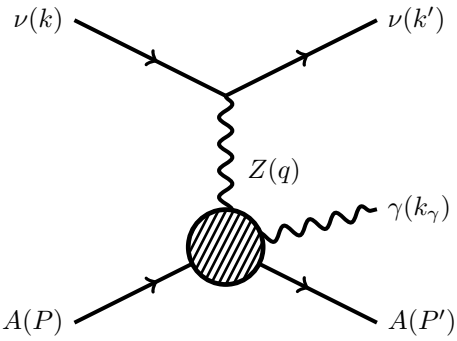


Fig. 13. Diagram for coherent photon emission induced by neutral currents.

where

$$L_{\mu\nu} = 8\left[k'_\mu\, k_\nu + k'_\nu\, k_\mu - g_{\mu\nu}(k'\cdot k) \pm i\epsilon^{\mu\nu\sigma\rho}k'_\sigma k_\rho\right] \tag{9}$$

is the standard leptonic tensor, and

$$R^{\mu\alpha} = \sum_{N=p,n} \frac{1}{2}\mathrm{Tr}\left[\frac{\not{p}+m_N}{2m_N}\gamma_0 \Gamma_N^{\mu\alpha}\right]\frac{m_N}{E_p}F_N\left(\left|\vec{q}-\vec{k}_\gamma\right|\right)\,, \tag{10}$$

in terms of the amputated amplitudes $\Gamma_N^{\mu\alpha}$ corresponding to the $Z\,N \to N\,\gamma$ matrix elements:

$$\langle N\gamma|\, J^\mu_{\mathrm{NC}\gamma}\,|ZN\rangle = \overline{u}\,(p')\,\Gamma_N^{\mu\alpha}u\,(p)\,\epsilon^*_\alpha\,(k_\gamma)\,, \tag{11}$$

with $\epsilon_\alpha(k_\gamma)$ the polarization of the outgoing photon. The nuclear form factors F_N arise as the Fourier transform of $\rho_{p,n}(r)$

$$F_N\left(\left|\vec{q}-\vec{k}_\gamma\right|\right) = \int d^3r\, e^{i(\vec{q}-\vec{k}_\gamma)\vec{r}}\,\rho_N(\vec{r}) \tag{12}$$

once the amputated amplitudes are evaluated at the average nuclear density and factorized out of the integration over $\vec{r}$. For the so far undefined nucleon momenta, we assume that the momentum transferred to the nucleus is equally shared by initial and final on-shell nucleons, so that $p = (E_p, \vec{p})$ with $\vec{p} = (\vec{k}_\gamma - \vec{q})/2$ and $E_p = \sqrt{m_N^2 + \vec{p}^{\,2}}$. This prescription is justified in Ref. [46], where it is also shown how the sum over nucleon helicities together with the choice of nucleon momenta leads to the trace in Eq. 10.

The elementary $ZN \to N\gamma$ amplitude includes the same mechanisms discussed above and represented by the Feynman diagrams of Fig. 8. In the case of the coherent process, nucleon-pole contributions are negligible; π and ρ exchange terms are not only small but, in the coherent case, vanish exactly for isospin symmetric nuclei. The ω exchange contribution, instead, does not vanish for symmetric nuclei because amplitudes on protons and neutrons add up rather than subtract. This mechanism was found subdominant at $E_\nu \sim 1$ GeV [34, 47]. Its relevance at higher energies is highly uncertain due to a high sensitivity to unknown form factors and unitarity constraints but cannot be discarded, due to its strong energy dependence [47], and deserves future studies. Here we focus on the contribution from baryon-resonance (N^* and Δ) intermediate states. The calculation of Ref. [36] considered $\Delta(1232)$, $N(1440)$, $N(1520)$ and $N(1535)$ intermediate states. Keeping in mind that there are experiments which work with higher energy fluxes, like MINERνA, where the medium-energy flux peaks

at around 6 GeV and can detect photons with energies above 500 MeV, we have extended the validity of the model to this domain [48]. This is done by adding to the amplitude new resonant diagrams for all the N^* and Δ states with invariant masses $W < 2$ GeV whose electromagnetic helicity amplitudes, upon which we rely, were extracted with the Mainz Unitary Isobar model (MAID) [49, 50].

Nuclear medium modifications of the resonant elementary amplitudes are neglected for all the states except the $\Delta(1232)$, which dominates the cross section and is known to be strongly modified in this medium. This is done by changing the $\Delta \to N\pi$ decay width to account for the Pauli blocking of the final nucleon and introducing an average broadening of twice the spreading potential $V_0 = 80$ MeV [39]. The obtained results are consistent with those obtained with the more sophisticated self-energy of Ref. [41].

In Fig 14 (left) the E_γ distributions are shown at 1, 3 and 6 GeV of incoming neutrino energy. The tendency of the cross section towards saturation is apparent, with small differences between the results at 3 and 6 GeV. These plots clearly show the dominant role of the $\Delta(1232)$. Some strength comes also from $N(1520)$ for $E_\gamma < 1$ GeV. For $E_\gamma > 1$ GeV, several resonances overlap but the only non negligible strength is provided by $\Delta(1700)$ and $\Delta(1950)$. Angular distributions, Fig. 14 (right), are forward

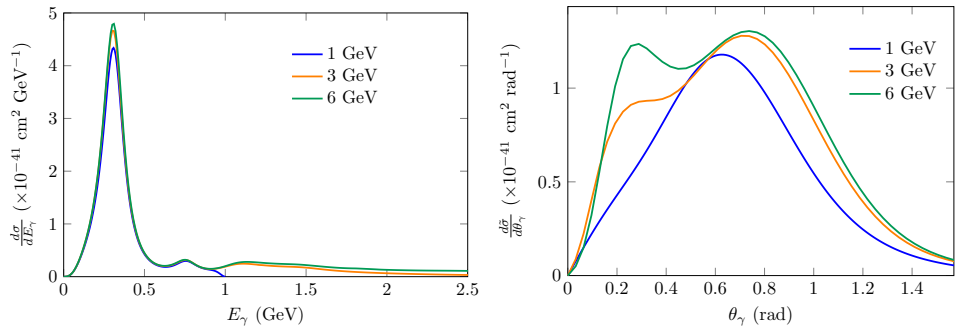


Fig. 14. Photon energy (left) and angular (right) distributions for coherent NCγ on ^{12}C for 1 GeV, 3 GeV and 6 GeV incoming neutrinos. For the angular distributions, only photon energies $E_\gamma < 2.5$ GeV have been considered.

peaked as expected for coherent scattering. As the neutrino energy increases, more strength is accumulated at small photon angles. For high energy photons, a small change in the angle will be highly disfavored by the nuclear form factor. As a consequence, the forward peak at around 0.2 rad in Fig. 14 (right) is a reflection of the contribution of the high energy tail in the energy distribution.

4 Some possible explanations of the anomaly.

Neutrino oscillations. As anticipated in the introduction, the main hypothesis to explain short baseline anomalies has traditionally been, and remains to be, the existence of additional families of sterile neutrinos able to mix with the SM ones. In a combined fit within the two-neutrino oscillation model to the final results in both neutrino and antineutrino mode, MiniBooNE finds a good description of the data. The best-fit point $(\sin^2 2\theta, \Delta m^2) = (0.807, 0.043\,\mathrm{eV}^2)$ is favored with respect to the background-only fit, which has a 3×10^{-7} smaller χ^2 probability.

On the other hand, the MiniBooNE results should be considered in the global context of other limits and signals. It was early observed that a $3+1$ model with three active and one sterile neutrinos offers a poor compatibility between ν and $\bar{\nu}$ datasets and an even poorer one (0.0013%) between appearance and disappearance measurements [51]. A more recent study [52] also finds a strong tension between appearance (LSND and MiniBooNE) and disappearance (MINOS, IceCube) data, although in this case the tension is dominated by LSND. Models with more sterile-neutrino families offer more flexibility but, nonetheless, global analyses struggle to accommodate the MiniBooNE excess with the world oscillation data even in 3+2 and 3+1+1 [3] neutrino mixing schemes, as clearly seen in Fig. 15 taken from Ref. [53]. As discussed in Secs. 1 and 2,

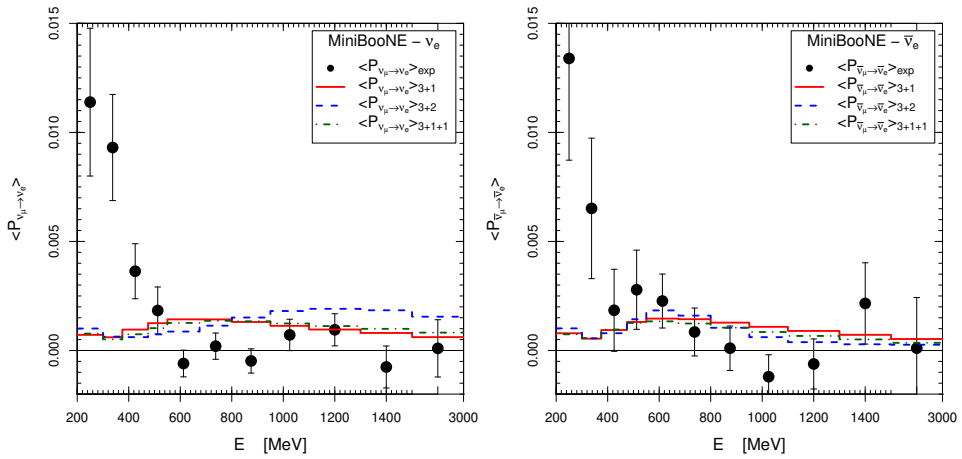


Fig. 15. Averaged transition probability in neutrino-energy bins corresponding to the best-fit values of the oscillation parameters in the 3+1, 3+2 and 3+1+1 fits [53] compared to the MiniBooNE excess data.

multinucleon interactions have an impact on the intrinsic ν_e ($\bar{\nu}_e$) background (Fig. 4) and introduce a bias in neutrino energy reconstruction. The consequences for global oscillation analyses were investigated in Ref. [18] with a 3+1 model. It was found that taking multinucleon interactions into account decreases the appearance-disappearance tension but is insufficient to remove it. In Ref. [54] it was estimated that the NC1γ background should be enhanced by a factor between 1.52 and 1.62 over the MiniBooNE estimate, depending on the energy range and mode. Such an enhancement, shrinks the excess and significantly reduces the appearance-disappearance tension in global fits but is at odds with the theoretical calculations of the NC1γ number of events at MiniBooNE described in Sec. 3. The upper limit for the NC1γ cross section recently obtained by the MicroBooNE experiment [**MicroBooNE:2021zai**] disfavors that the excess could be attributed to this reaction channel alone. The study of Ref. [**Brdar:2021cgb**] finds that the choice of event generator (NUANCE, GiBUU, GENIE, NuWro) has an impact on NCπ^0 and NC1γ backgrounds even when they are constrained by MiniBooNE's own data. The investigation of how the choice of event generator affects the fit in a $3+1$ model concludes that, even in the most favorable scenario, they seem unable to account for the anomaly.

[3] In the 3+1+1 scheme, the fifth neutrino is much heavier than 1 eV so that oscillations due to Δm^2_{51} are averaged [53].

Exotic mechanisms that can alter oscillations and eventually reconcile appearance and disappearance data have been proposed, and include Lorentz and CPT violation [57, 58], non-standard interactions [59], sterile neutrinos with modified dispersion relations [60], or a combination of oscillations and sterile neutrino decays [61–64]. In the following we consider some scenarios directly involving unconventional mechanisms of neutrino interactions at the detector leading to electron-like signals. The framework for global analyses of this kind of models has been presented in Ref. [65].

Production and radiative decay of heavy neutrinos. In an early study, Gninenko proposed that additional photons could originate in the weak production of a heavy ($m_h \approx 50$ MeV) sterile neutrino slightly mixed with muon neutrinos, followed by its radiative decay [66]. Following that, it was pointed out in Ref. [67] that the ν_h could also be electromagnetically produced, alleviating tensions in the original proposal with other data such as those from radiative muon capture measured at TRIUMF.

The scenario presented in Ref. [67] has been revisited using present understanding of electromagnetic (EM) and weak interactions on nucleons and nuclei [48]. The relevant processes are

$$\nu_\mu\,,\bar{\nu}_\mu(k)\;+\;N(p)\to\nu_h\,,\bar{\nu}_h(k')\;+\;N(p')\,, \tag{13}$$

$$\nu_\mu\,,\bar{\nu}_\mu(k)\;+\;A(p)\to\nu_h,\bar{\nu}_h(k')\;+\;A(p')\,, \tag{14}$$

$$\nu_\mu\,,\bar{\nu}_\mu(k)\;+\;A(p)\to\nu_h,\bar{\nu}_h(k')\;+\;X(p')\,, \tag{15}$$

followed by the decay of the heavy neutrino into a photon and a light neutrino, which could or could not be one of the SM flavors. Reaction (14) is coherent while (15) is incoherent; excited states X include any number of knocked out nucleons but no meson production. In the MiniBooNE case, the relevant targets are $N =$ proton and $A = {}^{12}\mathrm{C}$ ($\mathrm{CH_2}$).

In the case of an EM reaction in which an incoming light neutrino of flavor i turns into an outgoing heavy neutrino by single-photon exchange through a transition magnetic moment $\mu^i_{\rm tr}$, the most general effective interaction [68] leads to the effective Lagrangian proposed in Ref. [67]

$$\mathcal{L}_{\rm eff}\supset\frac{1}{2}\mu^i_{\rm tr}\left[\overline{\nu}_h\sigma_{\mu\nu}\left(1-\gamma_5\right)\nu_i+\overline{\nu}_i\sigma_{\mu\nu}\left(1+\gamma_5\right)\nu_h\right]\partial^\mu A^\nu\,. \tag{16}$$

In this scenario, the heavy neutrinos are Dirac particles with $m_{\nu_h}\gg m_{\nu_i}$. In the weak case, the neutrino vertex has the same structure as in the SM and is proportional to the mixing $U_{\mu h}$. The EM (NC) hadronic tensors are the same probed in the corresponding electron (neutrino) scattering processes. For the nucleon, it is given in terms of electromagnetic and axial form factors. For coherent scattering (14), the tensor is proportional to the square of the nuclear form factor. The incoherent reaction can be described with particle-hole excitations in infinite nuclear matter, adapted to finite nuclei using the local density approximation.

As shown in Fig. 16, with the set of parameters proposed in Ref. [67]: $m_h = 50$ MeV, $\mu^\mu_{tr} = 2.4\times10^{-9}\mu_B$ and $|U_{\mu h}|^2 = 0.003$, the EM cross section on nuclei is dominated by the coherent mechanism, while the incoherent one is suppressed by Pauli blocking at low four-momentum transfers, where the amplitude is enhanced by the photon propagator. On the contrary, the incoherent reaction is the largest contribution to the weak NC part. Interference terms between the EM and NC amplitudes are allowed but negligible.

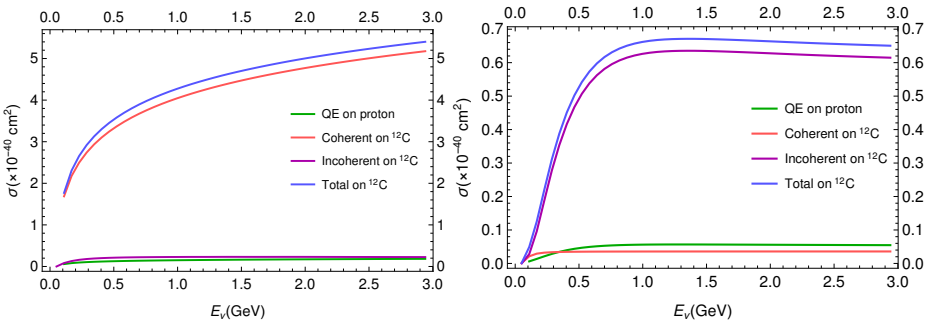


Fig. 16. Integrated cross sections for ν_h production in ν_μ-nucleus scattering by EM (left) and weak (right) interactions as a function of the incident neutrino energy.

The ν_h propagation and radiative decay inside the MiniBooNE detector has been investigated in Ref. [48]. We have taken advantage of the fact that, as pointed out in Ref. [67], the beam energies are large compared to m_h and only an insignificant amount of the electromagnetically (weakly) produced heavy neutrinos have the spin against (aligned with) its momentum. From the effective Lagrangian of Eq. 16 the angular distribution of the ν_h decay is found to be

$$\frac{d\Gamma}{d\cos\theta_\gamma}(\nu_h \to \nu_i + \gamma) = \frac{\left(\mu^i_{\rm tr}\right)^2 m_h^3}{32\pi}\left(1 \mp \cos\theta_\gamma\right) \ , \tag{17}$$

where the negative (positive) sign corresponds to the decay of left (right)-handed heavy neutrino; relatives signs are reversed for antineutrinos. This result implies that photons from radiative decays are emitted predominantly in the direction opposite to the ν_h spin and along the direction of the $\bar{\nu}_h$ spin [67]. In order to obtain the number of photon events in the detector and their angular and energy distributions one should further take into account that heavy neutrinos are produced with a scattering angle with respect to the incoming flux and travel a distance before their decay, which might occur outside the fiducial volume. Finally, to compare to the measured excess of events, the detection efficiency [43] has to be taken into account.

The model is constrained by four parameters: the heavy neutrino mass, m_h; the mixing angle between light and heavy neutrinos, U_{lh}; the heavy neutrino mean lifetime, τ_h, which is related to the magnetic dipole moment through Eq. 17, and the branching ratio of the ν_h decay to a light neutrino of flavor i, which depends on the corresponding transition magnetic moments, $\mathrm{BR}_i = \left(\mu^i_{\rm tr}\right)^2 / \sum_i \left(\mu^i_{\rm tr}\right)^2$.

With the parameters proposed in Ref. [67], the number of low energy events is underestimated in ν-mode, while the agreement is good in $\bar{\nu}$-mode. However, the predominantly EM coherent contribution is strongly forward peaked, leading to a very narrow angular distribution not observed in the experiment (see Fig. 2 of Ref. [69]). This result is in line with the findings of Ref. [70].

The agreement can be improved by fitting the parameters in the allowed range established in Ref. [71]. With values, $m_h = 70^{+10}_{-30}$ MeV, $\mathrm{BR}_\mu = 9^{+31}_{-9} \times 10^{-4}$, $|U_{\mu h}|^2 = 0.01$ and $\tau_h = 2.5^{+0.6}_{-1.2} \times 10^{-9}$ seconds, the resulting event energy and angular distributions are given in Fig. 17. The MiniBooNE excess of events is now better described, particularly the angular distributions. This is achieved at the price of reducing the EM strength, while increasing the NC one by setting $|U_{\mu h}|$ to its maximal allowed value: this upper limit in $|U_{\mu h}|$ prevents from obtaining a more satisfactory description of the data. More stringent bounds for $U_{\mu h}$ exist, in particular from radiative

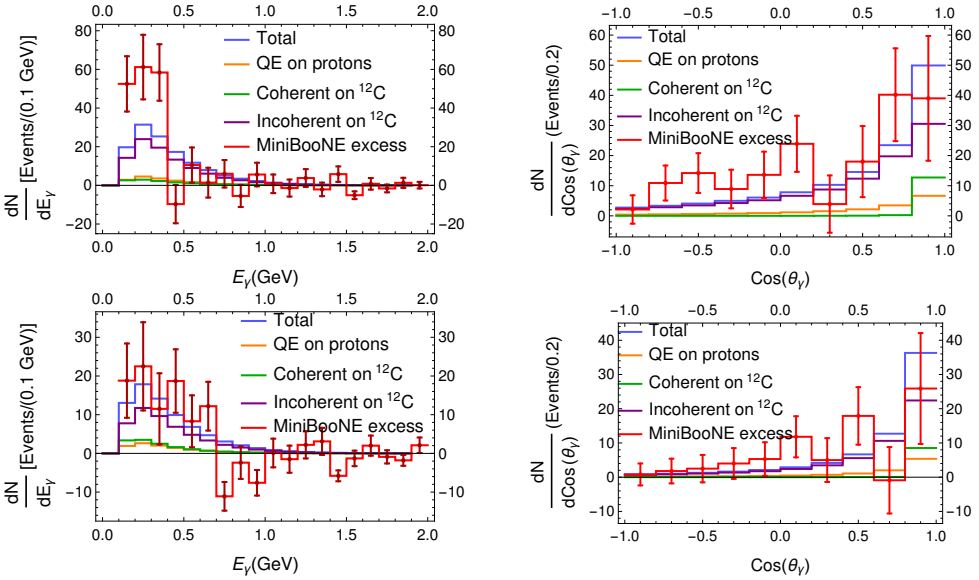


Fig. 17. Photon events from radiative decay of ν_h, $\bar{\nu}_h$ at the MiniBooNE detector in ν-mode (top) and $\bar{\nu}$-mode (bottom) compared to the MiniBooNE excess. The individual contributions of different ν_h production mechanisms are shown.

muon capture: $\mu^- p \to n \nu \gamma$, experimentally investigated at TRIUMF. The mixing upper bound from Ref. [72] is a decreasing function of m_h in the range under consideration (see Fig. 4 of Ref. [72]). Once the fit results are largely independent on the mass (Figure 4.16 of Ref. [48]) and improve for larger values of $U_{\mu h}$, we can set the mass to its allowed minimum of 40 MeV in order to have the largest possible upper bound in the mixing: $|U_{\mu h}|^2 = 8.4 \times 10^{-3}$. The fit with these new restrictions finds $\tau_h = 9.1^{+1.1}_{-1.5} \times 10^{-10}$ seconds, $\mathrm{BR}_\mu = 1.7^{+2.4}_{-1.4} \times 10^{-5}$ with a χ^2/DoF only slightly above the one for the previous fit.

The study outlined in this section shows that the hypothesis of Refs. [66, 67] cannot satisfactorily explain the MiniBooNE anomaly. In particular, there are clear difficulties to simultaneously describe the energy and the angular distributions of the electron-like events. Nevertheless, based on MiniBooNE data, radiative decay of heavy neutrinos cannot be fully excluded at least as a partial source of the excess. It is worth studying it further in the new generation of experiments at the Booster Neutrino Beam, which should be able to distinguish photons from electrons.

Production of sterile/dark neutrinos by beyond SM mediators. The previous scenario in which a heavy (but relatively light) neutrino is produced in interactions with SM mediators has the advantage that the hadronic/nuclear part of the interaction is either well known or can be further constrained with neutrino scattering on nucleons and nuclei. On the other hand, as illustrated above, SM constrains restrict our ability to explain the anomaly in this way. Stimulated by the MiniBooNE updates confirming the event excess, several generalizations and extensions that avoid some of the bounds have been recently put forward.

The basic idea of Ref. [73] is that heavy ($100 \lesssim m_h \lesssim 250$ MeV) sterile neutrinos are produced at the detector by NC interactions mediated by a new GeV-scale boson and subsequently decay into an e^+e^- pair misreconstructed as an electron. The new

boson, with a mass $m_{Z'} \gtrsim 1$ GeV is light enough to generate a large cross section with natural couplings and without the need of a large mixing $U_{\mu h}$, but heavy enough to elude the unrealistically narrow angular distribution that results in EM interactions. Interactions are built by extending the SM group with a $U(1)'$ gauge symmetry assumed to be broken at low energies. The low energy Lagrangian is [73]

$$\mathcal{L} = \mathcal{L}_{\nu\mathrm{SM}} - \frac{1}{4} X_{\mu\nu} X^{\mu\nu} - \frac{\sin\chi}{2} X_{\mu\nu} B^{\mu\nu} + \frac{\mu^2}{2} X_\mu X^\mu \,;$$

$\mathcal{L}_{\nu\mathrm{SM}}$ denotes an extension of the SM incorporating neutrino masses. The third term accounts for kinetic mixing characterized by the χ parameter; $F_{\mu\nu} \equiv \partial_\mu F_\nu - \partial_\mu F_\nu$ where F_μ stands for B_μ the SM $U(1)_Y$ gauge field, and X_μ for the $U(1)'$ one with mass μ from symmetry breaking. The kinetic mixing term between B_μ and X_μ can be removed by a field redefinition, identifying, after a change of basis, the states with definite mass with the photon, Z and Z' bosons. The coupling between SM fermions and the Z' is purely vector and proportional to both χ and the particle electric charge. SM-gauge singlets, which are charged under U(1)$'$, are introduced and mixed with the SM neutrinos. Therefore, one can have Z'-mediated $\nu_i \leftrightarrow \nu_h$ transitions

$$\mathcal{L} \supset U^*_{ih} g' \overline{\nu_i} \gamma^\mu (1 - \gamma_5) \nu_h \, Z'_\mu + \text{h.c.}\,, \tag{18}$$

responsible for both the ν_h production in the scattering of incoming neutrinos off the target nuclei and its subsequent decay $\nu_h \to \nu_i \, Z' \to \nu_i \, e^+ \, e^-$. In Ref. [73], coherent scattering off ^{12}C and incoherent scattering off constituent protons are considered but no medium corrections are applied to the later.

The shape of the visible energy and angular distributions of the MiniBooNE excess are well described, as illustrated in Fig. 18 for typical $m_h = 140$ MeV and $m_{Z'} = 1.25$ GeV. The total number of events depends meanly on χ and the mixing angles. In

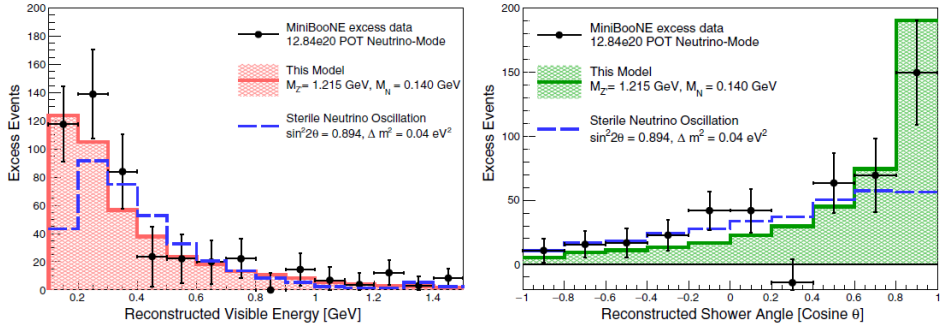


Fig. 18. Model predictions of Ref. [73] for the MiniBooNE event excess.

Fig. 18 the authors of Ref. [73] propose a minimal realization with $|U_{\mu h}|^2 = 1.5 \times 10^{-6}$, $|U_{\tau h}|^2 = 7.8 \times 10^{-4}$, $\chi^2 = 5 \times 10^{-6}$ and $g' = 1$. Notice that in this scenario, a good agreement with data does not require large mixing angles as in the much more constrained case of SM mediators discussed previously. It should be nonetheless noted that the large $|U_{\tau h}|^2$ (520 times larger than $|U_{\mu h}|^2$) would lead to sizable ν_h production rates in experiments with a large $\nu_\tau$component [74].

A successful explanation of the MiniBooNE anomaly is also obtained in Ref. [75] in a model similar to the one just described but with the assumption of $m_{Z'} < m_h$ (instead of $m_{Z'} > m_h$ in Ref. [73]) according to which the dark neutrino decays

into an on-shell Z'. In this case, the benchmark parameters are $m_h = 420$ MeV and $m_{Z'} = 30$ MeV, with a significantly lighter Z'. However, according to the simulation of Ref. [76], a model with such a light Z' would lead to a much narrower angular distribution of the event excess than the one observed by MiniBooNE. This is in line with the previously discussed EM (photon exchange) scenario.

These models, and variations including a larger number of heavy neutrinos [77] or scalar mediators [78, 79], can be tested by the Short Baseline program (SBN) at Fermilab whose liquid argon detectors (SBND, MicroBooNE and Icarus) can distinguish between electrons and photon or e^+e^- showers. The relevant parameter space can also be probed at MINERvA and CHARM-II [76]. The authors of Ref. [76] stress that in the case of MINERvA, such a study would benefit from theoretical calculations of coherent π^0 and single-photon emission more suitable at higher energies [above the $\Delta(1232)$]. The model described in Sec. 3 makes progress in this direction.

5 Outlook

The anomalous excess of events found by MiniBooNE remains an open problem that has puzzled physicists for over a decade. It may be a manifestation of still unknown sterile neutrinos or even new forces of nature. Its solution, therefore, has potential implications for the standing paradigm of neutrino and particle physics. On the other hand, an explanation related to unaccounted or poorly modeled backgrounds cannot yet be discarded, which calls for a better understanding of the interactions of few-GeV neutrinos with matter. New experimental information from the SBN program at Fermilab and the JSNS^2 at J-PARC but also from T2HK or DUNE will be priceless to close this chapter or, perhaps, open it wide.

Acknowledgements. We are indebted to Matheus Hostert and Teppei Katori for their valuable comments about the manuscript. This research has been partially supported by the Spanish Ministerio de Ciencia e Innovación under contracts FIS2017-84038-C2-1-P and PID2020-112777GB-I00, the EU STRONG-2020 project under the program H2020-INFRAIA-2018-1, grant agreement no. 824093 and by Generalitat Valenciana under contract PROMETEO/2020/023.

References

[1] A. Aguilar-Arevalo et al. "Evidence for neutrino oscillations from the observation of anti-neutrino(electron) appearance in a anti-neutrino(muon) beam". In: *Phys. Rev.* D64 (2001), p. 112007. DOI: 10.1103/PhysRevD.64.112007. arXiv: hep-ex/0104049 [hep-ex].

[2] P. A. Zyla et al. "Review of Particle Physics". In: *PTEP* 2020.8 (2020), p. 083C01. DOI: 10.1093/ptep/ptaa104.

[3] A. A. Aguilar-Arevalo et al. "The MiniBooNE Detector". In: *Nucl. Instrum. Meth. A* 599 (2009), pp. 28–46. DOI: 10.1016/j.nima.2008.10.028. arXiv: 0806.4201 [hep-ex].

[4] A.A. Aguilar-Arevalo et al. "The Neutrino Flux prediction at MiniBooNE". In: *Phys.Rev.* D79 (2009), p. 072002. DOI: 10.1103/PhysRevD.79.072002.

[5] A.A. Aguilar-Arevalo et al. "Improved Search for $\bar{\nu}_\mu \to \bar{\nu}_e$ Oscillations in the MiniBooNE Experiment". In: *Phys.Rev.Lett.* 110 (2013), p. 161801. DOI: 10.1103/PhysRevLett.110.161801.

[6] A. A. Aguilar-Arevalo et al. "Updated MiniBooNE neutrino oscillation results with increased data and new background studies". In: *Phys. Rev. D* 103.5 (2021), p. 052002. DOI: 10.1103/PhysRevD.103.052002. arXiv: 2006.16883 [hep-ex].

[7] Ulrich Mosel. "Neutrino event generators: foundation, status and future". In: *J. Phys. G* 46.11 (2019), p. 113001. DOI: 10.1088/1361-6471/ab3830. arXiv: 1904.11506 [hep-ex].

[8] Natalie Jachowicz, Nils Van Dessel, and Alexis Nikolakopoulos. "Low-energy neutrino scattering in experiment and astrophysics". In: *J. Phys. G* 46.8 (2019), p. 084003. DOI: 10.1088/1361-6471/ab25d4. arXiv: 1906.08191 [nucl-th].

[9] M. Martini, M. Ericson, and G. Chanfray. "Neutrino quasielastic interaction and nuclear dynamics". In: *Phys. Rev. C* 84 (2011), p. 055502. DOI: 10.1103/PhysRevC.84.055502. arXiv: 1110.0221 [nucl-th].

[10] J. Nieves, I. Ruiz Simo, and M. J. Vicente Vacas. "The nucleon axial mass and the MiniBooNE Quasielastic Neutrino-Nucleus Scattering problem". In: *Phys. Lett. B* 707 (2012), pp. 72–75. DOI: 10.1016/j.physletb.2011.11.061. arXiv: 1106.5374 [hep-ph].

[11] G. D. Megias et al. "Meson-exchange currents and quasielastic predictions for charged-current neutrino-^{12}C scattering in the superscaling approach". In: *Phys. Rev. D* 91.7 (2015), p. 073004. DOI: 10.1103/PhysRevD.91.073004. arXiv: 1412.1822 [nucl-th].

[12] A. Lovato et al. "Ab initio study of $(\boldsymbol{\nu_\ell}, \boldsymbol{\ell^-})$ and $(\boldsymbol{\bar{\nu}_\ell}, \boldsymbol{\ell^+})$ inclusive scattering in ^{12}C: confronting the MiniBooNE and T2K CCQE data". In: *Phys. Rev. X* 10.3 (2020), p. 031068. DOI: 10.1103/PhysRevX.10.031068. arXiv: 2003.07710 [nucl-th].

[13] M. Martini, M. Ericson, and G. Chanfray. "Energy reconstruction effects in neutrino oscillation experiments and implications for the analysis". In: *Phys. Rev. D* 87.1 (2013), p. 013009. DOI: 10.1103/PhysRevD.87.013009. arXiv: 1211.1523 [hep-ph].

[14] J. Nieves et al. "Neutrino Energy Reconstruction and the Shape of the CCQE-like Total Cross Section". In: *Phys. Rev. D* 85 (2012), p. 113008. DOI: 10.1103/PhysRevD.85.113008. arXiv: 1204.5404 [hep-ph].

[15] O. Lalakulich, U. Mosel, and K. Gallmeister. "Energy reconstruction in quasielastic scattering in the MiniBooNE and T2K experiments". In: *Phys. Rev. C* 86 (2012), p. 054606. DOI: 10.1103/PhysRevC.86.054606. arXiv: 1208.3678 [nucl-th].

[16] Teppei Katori. "MiniBooNE Neutrino Oscillation Search Results and Predicted Background Events". In: *3rd World Summit on Exploring the Dark Side of the Universe*. Oct. 2020. arXiv: 2010.06015 [hep-ex].

[17] G. Cheng et al. "Measurement of K^+ production cross section by 8 GeV protons using high energy neutrino interactions in the SciBooNE detector". In: *Phys. Rev. D* 84 (2011), p. 012009. DOI: 10.1103/PhysRevD.84.012009. arXiv: 1105.2871 [hep-ex].

[18] M. Ericson et al. "Assessing the role of nuclear effects in the interpretation of the MiniBooNE low-energy anomaly". In: *Phys. Rev. D* 93.7 (2016), p. 073008. DOI: 10.1103/PhysRevD.93.073008. arXiv: 1602.01390 [hep-ph].

[19] De-Liang Yao, Luis Alvarez-Ruso, and M. J. Vicente Vacas. "Neutral-current weak pion production off the nucleon in covariant chiral perturbation theory". In: *Phys. Lett. B* 794 (2019), pp. 109–113. DOI: 10.1016/j.physletb.2019.05.036. arXiv: 1901.00773 [hep-ph].

[20] T. Leitner et al. "Electron- and neutrino-nucleus scattering from the quasielastic to the resonance region". In: *Phys. Rev. C* 79 (2009), p. 034601. DOI: 10.1103/PhysRevC.79.034601. arXiv: 0812.0587 [nucl-th].

[21] S. X. Nakamura, H. Kamano, and T. Sato. "Dynamical coupled-channels model for neutrino-induced meson productions in resonance region". In: *Phys. Rev. D* 92.7 (2015), p. 074024. DOI: 10.1103/PhysRevD.92.074024. arXiv: 1506.03403 [hep-ph].

[22] E. Hernandez et al. "N-Delta(1232) axial form factors from weak pion production". In: *Phys. Rev. D* 81 (2010), p. 085046. DOI: 10.1103/PhysRevD.81.085046. arXiv: 1001.4416 [hep-ph].

[23] T. Leitner, L. Alvarez-Ruso, and U. Mosel. "Neutral current neutrino-nucleus interactions at intermediate energies". In: *Phys. Rev. C* 74 (2006), p. 065502. DOI: 10.1103/PhysRevC.74.065502. arXiv: nucl-th/0606058.

[24] Alexis A. Aguilar-Arevalo et al. "Measurement of ν_μ and $\bar{\nu}_\mu$ induced neutral current single π^0 production cross sections on mineral oil at $E_\nu \sim \mathcal{O}(1\text{GeV})$". In: *Phys. Rev. D* 81 (2010), p. 013005. DOI: 10.1103/PhysRevD.81.013005. arXiv: 0911.2063 [hep-ex].

[25] Olga Lalakulich and Ulrich Mosel. "Pion production in the MiniBooNE experiment". In: *Phys. Rev. C* 87.1 (2013), p. 014602. DOI: 10.1103/PhysRevC.87.014602. arXiv: 1210.4717 [nucl-th].

[26] Ulrich Mosel. "Pion Production in High-Energy Neutrino Reactions with Nuclei". In: *Phys. Rev. C* 91.6 (2015), p. 065501. DOI: 10.1103/PhysRevC.91.065501. arXiv: 1502.08032 [nucl-th].

[27] Callum Wilkinson et al. "Reanalysis of bubble chamber measurements of muon-neutrino induced single pion production". In: *Phys. Rev. D* 90.11 (2014), p. 112017. DOI: 10.1103/PhysRevD.90.112017. arXiv: 1411.4482 [hep-ex].

[28] A. A. Aguilar-Arevalo et al. "Measurement of ν_μ-induced charged-current neutral pion production cross sections on mineral oil at $E_\nu \in 0.5 - 2.0$ GeV". In: *Phys. Rev. D* 83 (2011), p. 052009. DOI: 10.1103/PhysRevD.83.052009. arXiv: 1010.3264 [hep-ex].

[29] B. Eberly et al. "Charged Pion Production in ν_μ Interactions on Hydrocarbon at $<E_\nu>= 4.0$ GeV". In: *Phys. Rev. D* 92.9 (2015), p. 092008. DOI: 10.1103/PhysRevD.92.092008. arXiv: 1406.6415 [hep-ex].

[30] U. Mosel and K. Gallmeister. "Muon-neutrino-induced charged current pion production on nuclei". In: *Phys. Rev. C* 96.1 (2017). [Addendum: Phys.Rev.C 99, 035502 (2019)], p. 015503. DOI: 10.1103/PhysRevC.96.015503. arXiv: 1708.04528 [nucl-th].

[31] Jan T. Sobczyk and Jakub Żmuda. "Investigation of recent weak single-pion production data". In: *Phys. Rev. C* 91.4 (2015), p. 045501. DOI: 10.1103/PhysRevC.91.045501. arXiv: 1410.7788 [nucl-th].

[32] C. T. Kullenberg et al. "A search for single photon events in neutrino interactions". In: *Phys. Lett. B* 706 (2012), pp. 268–275. DOI: 10.1016/j.physletb.2011.11.049. arXiv: 1111.3713 [hep-ex].

[33] K. Abe et al. "Search for neutral-current induced single photon production at the ND280 near detector in T2K". In: *J. Phys. G* 46.8 (2019), 08LT01. DOI: 10.1088/1361-6471/ab227d. arXiv: 1902.03848 [hep-ex].

[34] Richard J. Hill. "Low energy analysis of nu N —> nu N gamma in the Standard Model". In: *Phys. Rev. D* 81 (2010), p. 013008. DOI: 10.1103/PhysRevD.81.013008. arXiv: 0905.0291 [hep-ph].

[35] Brian D. Serot and Xilin Zhang. "Neutrinoproduction of Photons and Pions From Nucleons in a Chiral Effective Field Theory for Nuclei". In: *Phys. Rev. C* 86 (2012), p. 015501. DOI: 10.1103/PhysRevC.86.015501. arXiv: 1206.3812 [nucl-th].

[36] E. Wang, L. Alvarez-Ruso, and J. Nieves. "Photon emission in neutral current interactions at intermediate energies". In: *Phys. Rev. C* 89.1 (2014), p. 015503. DOI: 10.1103/PhysRevC.89.015503. arXiv: 1311.2151 [nucl-th].

[37] Jeffrey A. Harvey, Christopher T. Hill, and Richard J. Hill. "Anomaly mediated neutrino-photon interactions at finite baryon density". In: *Phys. Rev. Lett.* 99 (2007), p. 261601. DOI: 10.1103/PhysRevLett.99.261601. arXiv: 0708.1281 [hep-ph].

[38] Jonathan L. Rosner. "Low-energy photon production in neutrino neutral-current interactions". In: *Phys. Rev. D* 91.9 (2015), p. 093001. DOI: 10.1103/PhysRevD.91.093001. arXiv: 1502.01704 [hep-ph].

[39] Xilin Zhang and Brian D. Serot. "Incoherent Neutrinoproduction of Photons and Pions in a Chiral Effective Field Theory for Nuclei". In: *Phys. Rev. C* 86 (2012), p. 035502. DOI: 10.1103/PhysRevC.86.035502. arXiv: 1206.6324 [nucl-th].

[40] Xilin Zhang and Brian D. Serot. "Can neutrino-induced photon production explain the low energy excess in MiniBooNE?" In: *Phys. Lett. B* 719 (2013), pp. 409–414. DOI: 10.1016/j.physletb.2013.01.057. arXiv: 1210.3610 [nucl-th].

[41] E. Oset and L. L. Salcedo. "Δ Selfenergy in Nuclear Matter". In: *Nucl. Phys. A* 468 (1987), pp. 631–652. DOI: 10.1016/0375-9474(87)90185-0.

[42] E. Wang, L. Alvarez-Ruso, and J. Nieves. "Single photon events from neutral current interactions at MiniBooNE". In: *Phys. Lett. B* 740 (2015), pp. 16–22. DOI: 10.1016/j.physletb.2014.11.025. arXiv: 1407.6060 [hep-ph].

[43] MiniBooNE Collaboration. https://www-boone.fnal.gov/for_physicists/data_release/.

[44] G. Chanfray and M. Ericson. "γ production in neutrino interactions with nuclei". In: *Phys. Rev. C* 104.1 (2021), p. 015203. DOI: 10.1103/PhysRevC.104.015203.

[45] L. Alvarez-Ruso et al. "Charged current neutrino induced coherent pion production". In: *Phys. Rev. C* 75 (2007). [Erratum: Phys.Rev.C 80, 019906 (2009)], p. 055501. DOI: 10.1103/PhysRevC.75.055501. arXiv: nucl-th/0701098.

[46] J. E. Amaro et al. "Theoretical study of neutrino-induced coherent pion production off nuclei at T2K and MiniBooNE energies". In: *Phys. Rev. D* 79 (2009), p. 013002. DOI: 10.1103/PhysRevD.79.013002. arXiv: 0811.1421 [hep-ph].

[47] Xilin Zhang and Brian D. Serot. "Coherent Neutrinoproduction of Photons and Pions in a Chiral Effective Field Theory for Nuclei". In: *Phys. Rev. C* 86 (2012), p. 035504. DOI: 10.1103/PhysRevC.86.035504. arXiv: 1208.1553 [nucl-th].

[48] E. Saúl-Sala. "Open Problems in the Physics of Neutrino Interactions with Nucleons and Nuclei". https://ific.uv.es/nucth/Thesis_Saul_Sala.pdf. PhD thesis. Universidad de Valencia, Jan. 2021.

[49] D. Drechsel, S. S. Kamalov, and L. Tiator. "Unitary Isobar Model - MAID2007". In: *Eur. Phys. J. A* 34 (2007), pp. 69–97. DOI: 10.1140/epja/i2007-10490-6. arXiv: 0710.0306 [nucl-th].

[50] L. Tiator et al. "Electromagnetic Excitation of Nucleon Resonances". In: *Eur. Phys. J. ST* 198 (2011), pp. 141–170. DOI: 10.1140/epjst/e2011-01488-9. arXiv: 1109.6745 [nucl-th].

[51] Janet M. Conrad, William C. Louis, and Michael H. Shaevitz. "The LSND and MiniBooNE Oscillation Searches at High Δm^2". In: *Ann. Rev. Nucl. Part. Sci.* 63 (2013), pp. 45–67. DOI: 10.1146/annurev-nucl-102711-094957. arXiv: 1306.6494 [hep-ex].

[52] Mona Dentler et al. "Updated Global Analysis of Neutrino Oscillations in the Presence of eV-Scale Sterile Neutrinos". In: *JHEP* 08 (2018), p. 010. DOI: 10.1007/JHEP08(2018)010. arXiv: 1803.10661 [hep-ph].

[53] C. Giunti et al. "Pragmatic View of Short-Baseline Neutrino Oscillations". In: *Phys. Rev. D* 88 (2013), p. 073008. DOI: 10.1103/PhysRevD.88.073008. arXiv: 1308.5288 [hep-ph].

[54] C. Giunti, A. Ioannisian, and G. Ranucci. "A new analysis of the MiniBooNE low-energy excess". In: *JHEP* 11 (2020). [Erratum: JHEP 02, 078 (2021)], p. 146. DOI: 10.1007/JHEP11(2020)146. arXiv: 1912.01524 [hep-ph].

[55] P. Abratenko et al. "Search for Neutrino-Induced Neutral Current Δ Radiative Decay in MicroBooNE and a First Test of the MiniBooNE Low Energy Excess Under a Single-Photon Hypothesis". In: (Oct. 2021). arXiv: 2110.00409 [hep-ex].

[56] Vedran Brdar and Joachim Kopp. "An Altarelli Cocktail for the MiniBooNE Anomaly?" In: (Sept. 2021). arXiv: 2109.08157 [hep-ph].

[57] Teppei Katori, V. Alan Kostelecky, and Rex Tayloe. "Global three-parameter model for neutrino oscillations using Lorentz violation". In: *Phys. Rev. D* 74 (2006), p. 105009. DOI: 10.1103/PhysRevD.74.105009. arXiv: hep-ph/0606154.

[58] Jorge S. Diaz and Alan Kostelecky. "Lorentz- and CPT-violating models for neutrino oscillations". In: *Phys. Rev. D* 85 (2012), p. 016013. DOI: 10.1103/PhysRevD.85.016013. arXiv: 1108.1799 [hep-ph].

[59] Jiajun Liao and Danny Marfatia. "Impact of nonstandard interactions on sterile neutrino searches at IceCube". In: *Phys. Rev. Lett.* 117.7 (2016), p. 071802. DOI: 10.1103/PhysRevLett.117.071802. arXiv: 1602.08766 [hep-ph].

[60] Gabriela A Barenboim et al. "Sterile neutrinos with altered dispersion relations revisited". In: *JHEP* 03 (2020), p. 070. DOI: 10.1007/JHEP03(2020)070. arXiv: 1911.02329 [hep-ph].

[61] M. H. Moulai et al. "Combining Sterile Neutrino Fits to Short Baseline Data with IceCube Data". In: *Phys. Rev. D* 101.5 (2020), p. 055020. DOI: 10.1103/PhysRevD.101.055020. arXiv: 1910.13456 [hep-ph].

[62] Mona Dentler et al. "Decaying Sterile Neutrinos and the Short Baseline Oscillation Anomalies". In: *Phys. Rev. D* 101.11 (2020), p. 115013. DOI: 10.1103/PhysRevD.101.115013. arXiv: 1911.01427 [hep-ph].

[63] André de Gouvêa et al. "On The Decaying-Sterile Neutrino Solution to the Electron (Anti)Neutrino Appearance Anomalies". In: *JHEP* 07 (2020), p. 141. DOI: 10.1007/JHEP07(2020)141. arXiv: 1911.01447 [hep-ph].

[64] Stefano Vergani et al. "Explaining the MiniBooNE Excess Through a Mixed Model of Oscillation and Decay". In: (May 2021). arXiv: 2105.06470 [hep-ph].

[65] Vedran Brdar, Oliver Fischer, and Alexei Yu. Smirnov. "Model-independent bounds on the nonoscillatory explanations of the MiniBooNE excess". In: *Phys. Rev. D* 103.7 (2021), p. 075008. DOI: 10.1103/PhysRevD.103.075008. arXiv: 2007.14411 [hep-ph].

[66] S. N. Gninenko. "The MiniBooNE anomaly and heavy neutrino decay". In: *Phys. Rev. Lett.* 103 (2009), p. 241802. DOI: 10.1103/PhysRevLett.103.241802. arXiv: 0902.3802 [hep-ph].

[67] Manuel Masip, Pere Masjuan, and Davide Meloni. "Heavy neutrino decays at MiniBooNE". In: *JHEP* 01 (2013), p. 106. DOI: 10.1007/JHEP01(2013)106. arXiv: 1210.1519 [hep-ph].

[68] C. Broggini, C. Giunti, and A. Studenikin. "Electromagnetic Properties of Neutrinos". In: *Adv. High Energy Phys.* 2012 (2012), p. 459526. DOI: 10.1155/2012/459526. arXiv: 1207.3980 [hep-ph].

[69] Luis Alvarez-Ruso and Eduardo Saul-Sala. "Radiative decay of heavy neutrinos at MiniBooNE and MicroBooNE". In: *Prospects in Neutrino Physics*. Apr. 2017. arXiv: 1705.00353 [hep-ph].

[70] Alexander Radionov. "Constraints on electromagnetic properties of sterile neutrinos from MiniBooNE results". In: *Phys. Rev. D* 88.1 (2013), p. 015016. DOI: 10.1103/PhysRevD.88.015016. arXiv: 1303.4587 [hep-ph].

[71] Sergei N. Gninenko. "A resolution of puzzles from the LSND, KARMEN, and MiniBooNE experiments". In: *Phys. Rev. D* 83 (2011), p. 015015. DOI: 10.1103/PhysRevD.83.015015. arXiv: 1009.5536 [hep-ph].

[72] David McKeen and Maxim Pospelov. "Muon Capture Constraints on Sterile Neutrino Properties". In: *Phys. Rev. D* 82 (2010), p. 113018. DOI: 10.1103/PhysRevD.82.113018. arXiv: 1011.3046 [hep-ph].

[73] Peter Ballett, Silvia Pascoli, and Mark Ross-Lonergan. "U(1)' mediated decays of heavy sterile neutrinos in MiniBooNE". In: *Phys. Rev. D* 99 (2019), p. 071701. DOI: 10.1103/PhysRevD.99.071701. arXiv: 1808.02915 [hep-ph].

[74] Peter Ballett, Matheus Hostert, and Silvia Pascoli. "Dark Neutrinos and a Three Portal Connection to the Standard Model". In: *Phys. Rev. D* 101.11 (2020), p. 115025. DOI: 10.1103/PhysRevD.101.115025. arXiv: 1903.07589 [hep-ph].

[75] Enrico Bertuzzo et al. "Dark Neutrino Portal to Explain MiniBooNE excess". In: *Phys. Rev. Lett.* 121.24 (2018), p. 241801. DOI: 10.1103/PhysRevLett.121.241801. arXiv: 1807.09877 [hep-ph].

[76] Carlos A. Argüelles, Matheus Hostert, and Yu-Dai Tsai. "Testing New Physics Explanations of the MiniBooNE Anomaly at Neutrino Scattering Experiments". In: *Phys. Rev. Lett.* 123.26 (2019), p. 261801. DOI: 10.1103/PhysRevLett.123.261801. arXiv: 1812.08768 [hep-ph].

[77] Asli Abdullahi, Matheus Hostert, and Silvia Pascoli. "A dark seesaw solution to low energy anomalies: MiniBooNE, the muon (g-2), and BaBar". In: *Phys. Lett. B* 820 (2021), p. 136531. DOI: 10.1016/j.physletb.2021.136531. arXiv: 2007.11813 [hep-ph].

[78] Alakabha Datta, Saeed Kamali, and Danny Marfatia. "Dark sector origin of the KOTO and MiniBooNE anomalies". In: *Phys. Lett. B* 807 (2020), p. 135579. DOI: 10.1016/j.physletb.2020.135579. arXiv: 2005.08920 [hep-ph].

[79] Waleed Abdallah, Raj Gandhi, and Samiran Roy. "Understanding the MiniBooNE and the muon and electron $g-2$ anomalies with a light Z' and a second Higgs doublet". In: *JHEP* 12 (2020), p. 188. DOI: 10.1007/JHEP12(2020)188. arXiv: 2006.01948 [hep-ph].